NASA TECHNICAL TRANSLATION NASA TT-20089

MECHANICAL CHARACTERISTICS OF FILAMENT-WOUND PRESSURE VESSEL (BURST PRESSURE)

IN-37
97317
12P.

H. Iida, M. Uemura

Translation of "FW Atsuryokuyookino Rikigakutekitokusei (Taiatsu Kyoodo)" Japan Society for Aeronautical and Space Sciences, Journal (ISSN 0021-4663), vol. 33, no. 381, 1985, p.592-600

(NASA-TT-20089) MECHANICAL CHARACTERISTICS OF FILAMENT-WOUND PRESSURE VESSEL (BURST PRESSURE) (NASA) 22 p Avail: NTIS MC A02/MF A01 CSCL 13I N87-28021
G5/37 Unclas 0097317

NATIONAL AERONAUTICS AND SPACE ADMINISTRATION
WASHINGTON, D.C. 20546 JULY 1987

Report Documentation Page

1. Report No.	2. Government Accession No.	3. Recipient's Catalog No.
NASA TT-20089		

4. Title and Subtitle	5. Report Date
MECHANICAL CHARACTERISTICS OF FILAMENT-WOUND PRESSURE VESSEL (BURST PRESSURE)	July 1987
	6. Performing Organization Code

7. Author(s)	8. Performing Organization Report No.
H. Iida, M. Uemura	
	10. Work Unit No.

9. Performing Organization Name and Address	11. Contract or Grant No.
Leo Kanner Associates Redwood CIty, CA 94063	NASW-4005
	13. Type of Report and Period Covered
12. Sponsoring Agency Name and Address National AEronautics and Space Administration Washington, DC 20546	Translation
	14. Sponsoring Agency Code

15. Supplementary Notes

TRanslation of "FW Atsuryokuyookino Rikigakuteki Tokusei (Taiatsu Kyoodo)" Japan Society for Aeronautical and Space Sciences, Journal (ISSN 0021-4663), vol. 33, no 381, 1985, pp. 592-600
86A25235

16. Abstract

The finite element method is used to analyze the mechanical characteristics of a pressurized filament-wound (FW) pressure vessel, and to predict its burst pressure. The analysis takes into account the bending moment, the stretch-bending coupling effect, nonlinear stress-strain relations, and finite deflection. The analysis is based on two initial failure criteria for laminae, and two ultimate fracture criteria for laminated structures. The numerical results, obtained by applying the load incremental method to the isotensoid CFRP pressure vessel used in the launching of the Zikiken satellite, are in good ageeement with the experimental burst pressure and fracture behaviors. I.S.

17. Key Words (Suggested by Author(s))	18. Distribution Statement
	Unclassified-Unlimited

19. Security Classif. (of this report)	20. Security Classif. (of this page)	21. No. of pages	22. Price
Unclassified	Unclassified	20	

NASA FORM 1626 OCT 86

MECHANICAL CHARACTERISTICS OF FILAMENT-WOUND PRESSURE VESSEL (BURST PRESSURE)

H. Iida, M. Uemura

1. Indroduction

The fiber reinforced plastic (FRP) has been popular for use in many areas of industrial materials. Particularly the application of FRP, made by use of the filament winding (FW) technique, on pressure vessels has been in the lime light because it has high specific tensil strength and stiffness along the fiber orientation and is suited for the formation of arbitrary convex shapes. However for designing the solid winding FW pressure vessels, only the ultimate fracture has been assumed and simple theories such as netting theory in which only the fibers are charge resistant, has been used in the past. In realty, the cracks along the fiber orientation from initial pressure occures and in the long run the initial failure should be considered.

Here, we analyzed the mechanical characteristics of solid winding FW pressure vessels before the initial failure using finite element technique taking into account the geometric nonlinear stretch-bending coupling effect. This analysis was in good agreement with experimental results of GFRP and CRFP pressure vessels 1-3). In the last report 4), on top of the nonlinear

shearing characteristics of one directional reinforced material in each layer. material nonlinearity due to unloading after the initial crack along the fiber orientation was considered. Then, the behavior of initial failure to ultimate fracture was analyzed using the finite element technique of the load incremental method based on the general laminated membrane theory. The initial failure occured near the aperature and explained the results of the experiment on the burst pressure and fracture behavior.

In this report, the analysis of the last report is improved. Based on laminated bending theory, instead of laminated film theory, we will introduce the analysis using the finite element technique which includes the mechanical and material nonlinear and coupling effect. In addition, the analysis was made with an effective assumption that unload behavior after the initial failure increases as the fracture advances. The numerical results on a CFRP pressure vessel which was used for the kick-motor EXOS-B were obtained and the burst structure in which the initial failure and the ultimate fracture occures near the aperture became clear. This became comparatively in good agreement with the experimental results on burst pressure and fracture behavior. /592

2. Analysis on burst pressure with geometrical and material nonlinear characteristics of FW rotary shell in consideration.

We will explain the burst pressure analysis thechnique to obtain the ultimate burst strength. Considering the FW pressure vessel as a rotary shell, this technique uses the laminated bending theory which takes into account the coupling effect together with geometrical and material nonlinear characteristics.

It presumes that λ which indicates unloading behavior after the initial failure increases along with the development of the fracture. at the quadratic function of strain.

2.1 Element characteristics.

A slice of a rotary shell perpendicular to the axis of symmetry. is divided into topless circular cone elements of half vertical angel ϕ. The distance on meridional direction from an element i is s. the radius is r. The displacement components of meridional direction. circumferencial direction θ and the direction perpendicular to the first two on the right side are u, v, w respectively. The incremental variation-displacement of solid winding layer central surface is exressed as the following, considering the large deflection.

$$\left.\begin{aligned}
&\Delta\varepsilon_s=\Delta u_{,s}+w_{,s}\Delta w_{,s}\\
&\Delta\varepsilon_\theta=(\Delta u\sin\phi+\Delta w\cos\phi)/r\\
&\Delta\gamma_{s\theta}=\Delta v_{,s}-\Delta v\sin\phi/r\\
&\Delta K_s=-\Delta w_{,ss}\\
&\Delta K_\theta=-\Delta w_{,s}\sin\phi/r\\
&\Delta K_{s\theta}=2\Delta v_{,s}\cos\phi/r-2\Delta v\cos\phi\sin\phi/r^2
\end{aligned}\right\} \qquad (1)$$

Suffix .s, .ss are derivatives of S. As for the relations of membrane force, moment -strain, curvature variations, the coupling effect between the inner stretch and bending from the Kirchhoff-Love Assumptions is considered and expressed in incremental shapes:

$$\begin{Bmatrix}\Delta N_s\\ \Delta N_\theta\\ \Delta N_{s\theta}\\ \hline \Delta M_s\\ \Delta M_\theta\\ \Delta M_{s\theta}\end{Bmatrix}=\left[\begin{array}{ccc:ccc}A_{11}&A_{12}&A_{13}&B_{11}&B_{12}&B_{13}\\ A_{12}&A_{22}&A_{23}&B_{12}&B_{22}&B_{23}\\ A_{13}&A_{23}&A_{33}&B_{13}&B_{23}&B_{33}\\ \hdashline B_{11}&B_{12}&B_{13}&D_{11}&D_{12}&D_{13}\\ B_{12}&B_{22}&B_{23}&D_{12}&D_{22}&D_{23}\\ B_{13}&B_{23}&B_{33}&D_{13}&D_{23}&D_{33}\end{array}\right]\times\begin{Bmatrix}\Delta\varepsilon_s\\ \Delta\varepsilon_\theta\\ \Delta\gamma_{s\theta}\\ \hline \Delta K_s\\ \Delta K_\theta\\ \Delta K_{s\theta}\end{Bmatrix} \qquad (2)$$

Aij, Bij and Dij of D matrix components are explained in the next

ORIGINAL PAGE IS
OF POOR QUALITY

chapter.

Assuming now that incremental strain energy for obtaining the stiffness matrix satisfies the equibrium equation already, 1 radian worth the circumference coordinates is obtained by the next equation.

$$\frac{1}{2}\int_0^L (\Delta N_s \Delta\varepsilon_s + \Delta N_\theta \Delta\varepsilon_\theta + \Delta N_{s\theta}\Delta\gamma_{s\theta} + \Delta M_s \Delta K_s + \Delta M_\theta \Delta K_\theta + \Delta M_{s\theta}\Delta K_{s\theta}) r\,ds + \int_0^L N_s^{(\omega)} \frac{1}{2}(\Delta w_{,s})^2 r\,ds \qquad (3)$$

L is an element length along the meridian direction, $N_s^{(\omega)}$ is the meridian membrane force in the former step, $(\Delta w_{,s})^2/2$ is the 2nd term which is ignored in the $\Delta\varepsilon_s$ equation of (1). The load incremental technique is used to bring in the geometrical nonlinear 3).

In a FW vessel, the winding angle of fiber to the meridian w and the thickness h varies in each position, depending on its dome shape and winding. For a Helical winding isotensoid curved vessel which we used in the experiment, fiber orientation is along the geodetic line, and expressed as:

$$\sin\omega = r_i/r \qquad (4)$$

$$h = h_o r_i \cos\omega_o / r\cos\omega \qquad (5)$$

r_i is aperature radius, h_o, r_o, w_o are values in the cylinder portion (dome bottom).

The isotensoid curved surface has the infinite curvature radius on meridian surface at $r=\sqrt{3/2}r_i$ point which is near the aperature, so the radii below that are circular cone shapes that connect smoothly. Nonlinear stress-strain relations and normal burst strength of one directional reinforced materials which are the fundamentals of FW pressure vessels were obtained by the

experiments 5,6). The results are explained in 3.1.

2.2 D matrix on the dome portion and the hoop winding reinforcement portion.

(1) Dome portion (Angle-ply layer).

FW pressure vessel with a helical winding isotensoid curve shape has the equally thick layer with an angle of intersection ±w of fiber to meridian, and is laminated in even reverse symmetry, and has m layers as shown in Fig. 1. Stress distribution in each layer was analyzed with nonlinear shearing stress-shearing strain relations along the fiber in consideration, to determine the initial failure. After that, stress-strain elastic modulus E_T or G_{LT}, which are based on a certain layer's fiber, decreases as internal pressure increases. λ which indicates unloading behavior after initial failure which is assumed by the quadratic function, will be explained in 2.3.

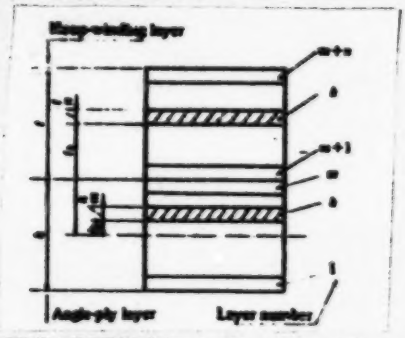

Fig. 1 Section view of layers including meridian.

593

For $\bar{E}_{ij}$ in connection with the dome's structual principal axis is an even function to w When ij=11,22,66,12, and an odd function when ij=16,26. So the coupling effect is in consideration, but in order to simplify the equ. which denotes the behavior after the initial failure, a lamina is made of a pair of angle-ply layers of ±w with +w as an inner layer, and the thickness of the whole laminate is h. Then D matrix components A_{ij}, B_{ij}, D_{ij} are:

ORIGINAL PAGE IS
OF POOR QUALITY

$$\left.\begin{aligned}&(A_{ij}, B_{ij}, D_{ij})\\&=\sum_{k=1}^{n} E_{ij}^{(k)}\frac{h}{m}\left(1,\ h_k+\frac{h}{2m},\right.\\&\left.h_k^2+h_k\frac{h}{m}+\frac{h^2}{3m^2}\right)\\&ij=11,\ 22,\ 66,\ 12\text{のとき}\\&(A_{ij}, B_{ij}, D_{ij})\\&=-\sum_{k=1}^{n} E_{ij}^{(k)}\frac{h^2}{4m^2}\left(0,\ 1,\ 2h_k+\frac{h}{m}\right)\\&ij=16,\ 26\text{のとき}\end{aligned}\right\} \quad (6)$$

h_k is the distance between the center of angle-ply layer to the inside surface of k-th layer.

(2) Central cylindrical portion (Angle-ply layer + hoop winding reinforcement layer).

The central cylindrical part and a portion of the dome on both sides is reinforced with a hoop parallel winding layer. Taking the differences between stress and strain on various thickness directions and the quadratic functional decrease of E_T or G_{LT} after initial failure into onsideration, the hoop parallel winding layer is divided into n layers along the thickness.

Hoop-winding layer $Ei_j^{(R)}$ is obtained by the $Ei_j^{(\omega)}$ equation with $\omega=90^\circ$. When the angle-ply layer of thickness h is laminated with a hoop-winding layer of thickness t, D matrix components of the central angle-ply layer are:

$$\left.\begin{aligned}&(A_{ij}, B_{ij}, D_{ij})\\&=\sum_{k=1}^{m\times n}\left\{E_{ij}^{(k)}\frac{h}{m}\left(1,\ h_k+\frac{h}{2m},\right.\right.\\&\left.h_k^2+h_k\frac{h}{m}+\frac{h^2}{3m^2}\right)\\&\left.+E_{ij}^{(k)}\frac{t}{n}\left(1, t_k+\frac{t}{2n}, t_k^2+t_k\frac{t}{n}+\frac{t^2}{3n^2}\right)\right\}\\&ij=11,\ 22,\ 66,\ 12\text{のとき}\\&(A_{ij}, B_{ij}, D_{ij})\\&=-\sum_{k=1}^{m\times n} E_{ij}^{(k)}\frac{h^2}{4m^2}\left(0,\ 1,\ 2h_k+\frac{h}{m}\right)\\&ij=16,\ 26\text{のとき}\end{aligned}\right\} \quad (7)$$

Here, t is a distance between the central angle-ply layer and k-th inner layer of hoop-winding layer.

2.3 Burst pressure.

The analysis of the behavior of the initial failure advancing to an ultimate fracture is made for a laminated rotary shell with the stretch bending coupling effect taken into consideration. We will list the criteria and the assumtions, now.

(1) Initial failure criteria.

For initial failure criteria of a laminated structure with fundermantal characteristics of the material which includes nonlinear shearing stress-strean relations of one directional reinforced material along the fiber, the ultimate stress theory is applied to the one directional reinforced layer which constructs the each layer.

$$\left.\begin{array}{l} \sigma_1 \geq F_1 \ (\sigma_1 > 0 \text{のとき}), \\ \sigma_2 \geq F_2 \ (\sigma_2 > 0 \text{のとき}), \\ \sigma_2 \leq -F_2' \ (\sigma_2 < 0 \text{のとき}), \\ |\tau_{12}| \geq F_{12} \end{array}\right\} \qquad (8)$$

Here, F_L : tensil strength along fiber, F_T : tensil strength perpendicular to fiber, F : pressure intensity perpendicular to fiber, F_T' : shearing strengh along fiber.

However, one directional reinforced material has $F_1 >> F_T$, F_T', F_{LT}, so there is no initial failure at F_L.

(2) Assumption of λ which denotes the unloading behavior after initial failure.

After initial failure at a one directional reinforced material layer, local cracks along the fiber occurs and grows into an ultimate fracture together with stress re-allotment. In the

last report 4) it was reported, even though quantatively unknown but in macroscopic view, λ which indicates unloading behavior, that after initial failure is 1 and gets larger as failure advances. In this report, λ is expressed by quadratic polynominal on ε_T . (ε_T)$_1$ is the strain perpendicular to the fiber at initial failure, λ_1 is λ which denotes the decreasing ratio of σ_T which occures with the increase of strain when σ_T=0, $d\lambda/d\varepsilon$ at initial failure is 0.

$$\lambda=1+\frac{1}{9}(\lambda_1-1)(\lambda_1+2)^2\frac{E_T^2}{F_T^2}(\varepsilon_T-(\varepsilon_T\lambda)^2 \quad (9)$$

The stress which is perpendicular to the fiber σ_T is denoted in the following equation using integral calculus on $-\lambda E_T$.

$$\sigma_T=F_T-E_T(\varepsilon_T-(\varepsilon_T\lambda)$$
$$\sim -\frac{1}{27}(\lambda_1-1)(\lambda_1+2)^2\frac{E_T^2}{F_T^2}(\varepsilon_T-(\varepsilon_T\lambda)^2 \quad (10)$$

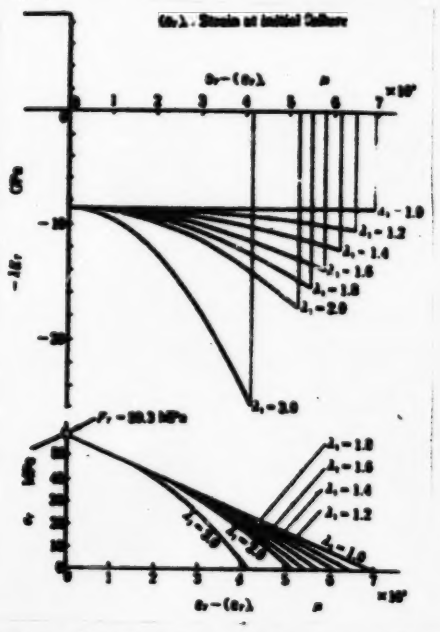

Fig. 2 Unloading behavior after initial failure.

Fig. 2 shows the values $-\lambda E_T$ and σ_T after intial failure, which are obtained from (9) and (10). After σ_T =0 then E_T=0 and the same λ is used for the Poison's ratio ν_T after initial failure. For shearing strength F_{LT} along the fiber after initial failure, it is predicted to have an unloading of τ_{LT}, and the same assumption as above is applied.

(3) Ultimate fracture criteria.

ORIGINAL PAGE IS
OF POOR QUALITY

Behavior of each layer after initial failure is calculated from the assumption (2) and when one of the fracture criteria occures, the FW pressure vessel of laminated material will be fractured.

① Fracture behavior by fiber deflection.

We considered the following equation when after the stress allotment, the increased stress along fiber reaches the limit. /594

$$\sigma_1 \geq F_1 \ (\sigma_1 > 0 \text{のとき}), \quad \text{または} \ \sigma_1 \leq -F_1' \ (\sigma_1 < 0 \text{のとき}) \qquad (11)$$

② Fracture behavior without fiber deflection.

We considered the following equation as the limit of the structural instability where determinant of D matrix reaches 0 and deformation and stress become unsettled.

$$\begin{vmatrix} A_{11} & A_{12} & A_{16} & B_{11} & B_{12} & B_{16} \\ A_{12} & A_{22} & A_{26} & B_{12} & B_{22} & B_{26} \\ A_{16} & A_{26} & A_{66} & B_{16} & B_{26} & B_{66} \\ B_{11} & B_{12} & B_{16} & D_{11} & D_{12} & D_{16} \\ B_{12} & B_{22} & B_{26} & D_{12} & D_{22} & D_{26} \\ B_{16} & B_{26} & B_{66} & D_{16} & D_{26} & D_{66} \end{vmatrix} \leq 0 \qquad (12)$$

3. Numerical values calculated on CFRP. FW rocket chamber.

3.1 The vessel shape, sizes and fundamental characteristics of material used.

Fig. 3 shows the shape, measurements and topless circular cone elements numbers. Solid helical winding layer (angle-ply layer) is a 6 layer laminae wound 3 times not parallel to the circumference. At the cylindrical portion, the thickness h_0=2.3mm, winding angle of fiber is constant and $w_0=\sin^{-1}(r_i/r_0)=24.9°$. The center of the cylinder is further more reinforced by laminating a hoop-winding layer (t_0=2.4mm) on top of the angle-ply layer. It is

ORIGINAL PAGE IS OF POOR QUALITY

ORIGINAL PAGE IS
OF POOR QUALITY

wound towards the dome for the width of 50.5mm on the meridian direction by decreasing its thickness.

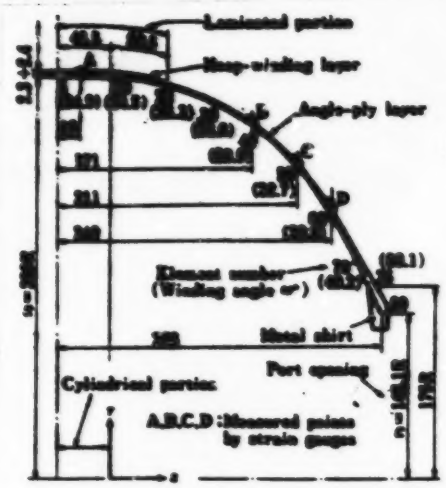

Fig. 3 Shape and measured points of CFRP isotensoid curved pressure vessel.

The results of the tension tests of one directional CFRP material along the fiber and perpendicular to it are shown in Fig. 4 (a), and (b). The stress-strain relation is linear until the fracture. The shearing stress-shearing strain relation is nonlinear as seen in FIg. 4 (c). 3rd spline interpolation function was used for the analysis. Table 1 shows the mean initial elastic modulus E_L, E_T, ν_L, G_{LT} and initial basic burst strength F_L, F_T, F_{LT}

3.2 Metal skirt at the aperture, its handling and the boundary conditions.

Assuming that the metal fitting Al alloy and CFRP material at the dome are bonded completely, the stiffness of the skirt between the CFRP laminated structure and the alloy was obtained using the laminated bending theory. For the boundary condition used in the finite element technique, displacement in the radius direction at the aperture and the rotation at the meridian was fixed; also the total load in the axis direction due to the internal pressure received at the cover of the aperture is the distributed load around the aperture.

TABLE 1 INITIAL ELASTIC MODULI AND [illegible] USED IN THE CALCULATIONS

		Init. elastic modulus (GPa)	Bend. strength (GPa)	Remarks
One directional CFRP material	Tension along fiber	E_1=135(ν_{12}=0.28)	R_1=1.96	Linear until break
	Tension perpend. to fiber	E_2=8.96	R_2=39.2	Linear until break
	Shearing along fiber	G_{12}=3.11	R_{12}=39.4	Interpolation with cubical spline curve
Metal skirt Al alloy		E=70.6(ν=0.29)		

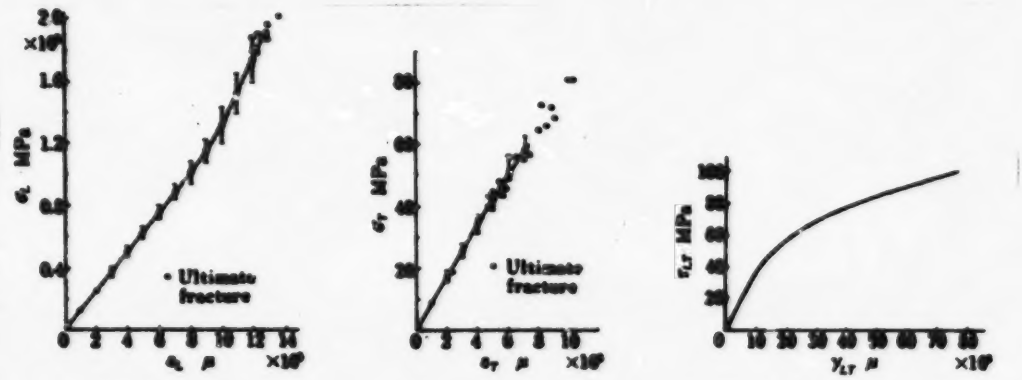

(a) Tension along fiber (b) Tension perpendicular to fiber (c) Shearing along fiber

Fig. 4 Tension and shearing characteristics of one directional reinforced CFRP.

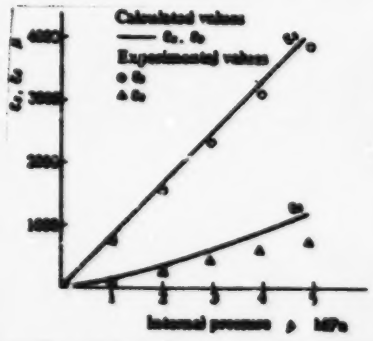

Fig. 5 Calculated and experimental values of internal pressure-outer layer strain, at B point, h_b=2.3mm (CFRP).

3.3 Calculated results and thoughts.

We used the load incremental method. Up to the initial faillure, the load increment is Δp=0.0539MPa, after the initial failure, it is Δp=0.0270MPa. As for λ, the unloading behavior after the initial failure, its quadric curve is obtained from Equ. (9) and (10), when the value λ_j, which shows the reduction ratio of σ_r as strain increases, is changed to 6 cases (see Fig.2). The following are the examples of the calculations.

ORIGINAL PAGE IS OF POOR QUALITY

ORIGINAL PAGE IS
OF POOR QUALITY

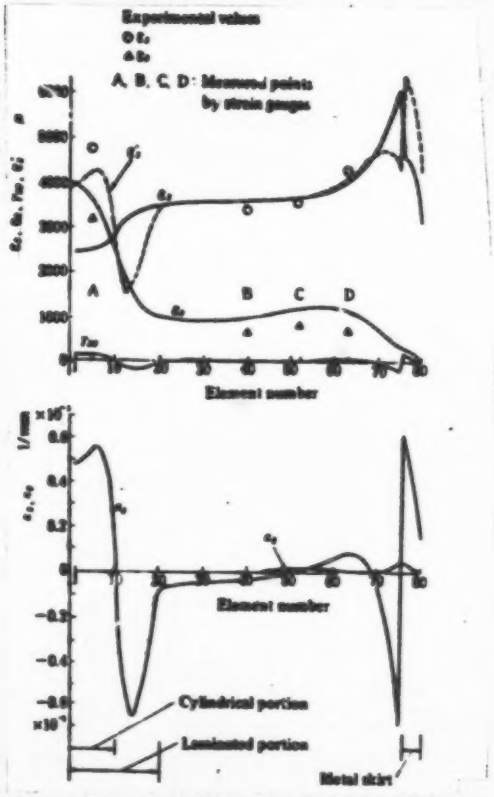

Fig. 6 Distributions of inner strain $\varepsilon_s, \varepsilon_\theta, \gamma_{s\theta}$, surface strain ε_s', curvature changes Ks, Kφ, and the comparison with the experimental values of surface strain. p=4.31MPa

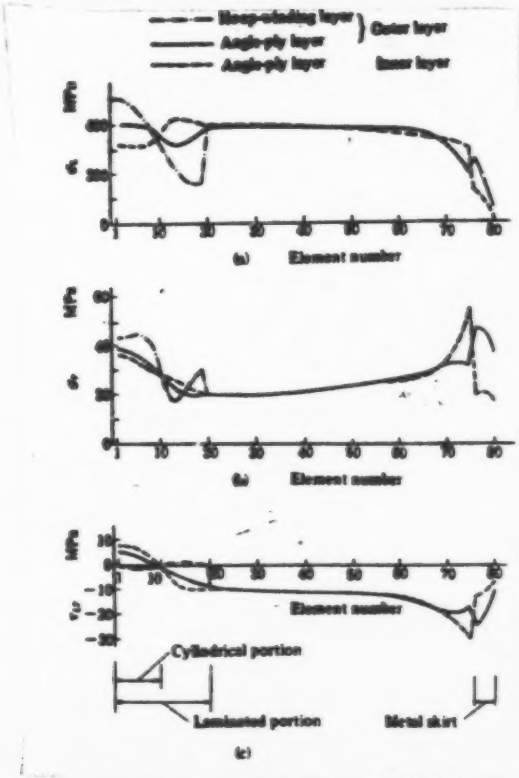

Fig. 7 Stress distributions $\sigma_L, \sigma_T, \tau_{LT}$ of inner and outer layers. p=4.31MPa

(1) Strain in structual axis direction and curvature change.

Nonlinear pressure-outer layer stress relation is obtaind by calculating up to the internal pressure before the initial failure is p=4.31MPa in 80 steps. One example at B point is shown in Fig.5.

Next, at internal pressure p=4.31MPa, strain in the structual axis direction ε_s, ε_θ, $\gamma_{s\theta}$, outer layer strain ε_c^0 and distribution of numerical values of curvature change Ks, K_θ are shown in Fig.6. /595

The strain along the meridian ε_s is comparatively constant near the dome, rapidly grows near the skirt because the winding angle w gets bigger, but it is small where the skirt is bonded

because of the reinforcement of the skirt, and is also small at the hoop winding superposed laminate area. Circumferencial strain ε_θ does not change much near the dome, but is small near the metal fitting because of the large w and effective skirt, and gets larger at the cylindrical portion as circumferencial strain increases. Shearing stress $\tau_{s\theta}$ occurs near the skirt and the hoop-winding superposed laminate area, but is small.

Curvature changes along meridian Ks, which was not considered in the last report 4), is small at the dome, and large near the metal fitting and hoop-winding superposed laminate where a bending moment occurs. Therefore, the distribution of the outer layer strain , which is different from the membrane strain , is indicated with the dotted line. K along the circumference is small.

(2) Distribution of stress on fiber criteria σ_L, σ_T, τ_{LT}

For the FW pressure vessels with internal pressure p=4.31MPa, bending moment occurs near the metal fitting and hoop-winding superposed laminate area. So the stress distributions based on the fiber of angle-ply inner and outer layers, hoop parallel winding outer layer σ_L, σ_T, τ_{LT} are shown as the broken, the streight and the dotted line, lide Fig.7 (a,b,c).

As seen in Fig.7 (a), the stress along fiber σ_L is quite small compared to F_L =1870NPa, σ_L is roughly the same at dome portion because of its isotensoid curved surface, is small at the metal skirt area because of the effective skirt, is large at the hoop-winding outer layer of central cylindrical area distributing the hoop stress. Stress perpendicular to fiber as seen in FIg.7 (b), σ_T is large at the cylindrical portion and the circumference of

596

the skirt, since the bending superposes there, and is close to Fr=59.3MPa and the initial failure occurs. Distribution of shearing stress γ_{LT} in Fig.7 (c), shows that it is small at the cylindrical portion, becomes large at the dome portion near the circumference of the skirt, but shearing falure does not occur since it is $|\gamma_{LT}|$<<99.6MPa.

(3) Stress changes and distribution of the inner layer in thickness direction of skirt circumference after initial failure.

It seems that as internal pressure intensifies, initial failure (F_r =59.3MPa) occurs at the internal pressure p =4.64MPa, then stress re-allocates, and ultimately falls into fracture. σ_r-internal pressure p relation and the final value of σ_r before fracture of the inner layer of the skirt circumference in 7 curves (λ_1=1.0-3.0) are shown in Fig. 8 and Table 2.

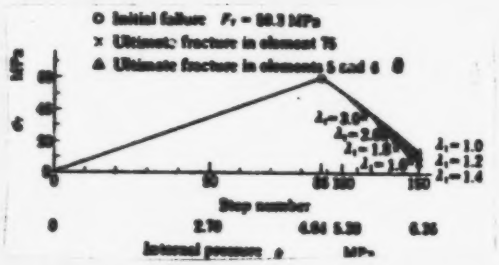

Fig. 8 Stress changes after initial failure of skirt circumference (element #75) inner 1st layer.

The stress σ_r of first inner layer of skirt circumference (element #75) reaches ultimate fracture at cylindrical portion (element 5, 6) when p=6.39MPa for λ_F1.0-1.4 (· Δ in Fig. 8), and for λ=1.6-3.0 when $-\lambda E_r$ lowers greatly it reaches ultimate fracture with lower inner pressure (x in Fig. 8). σ_t, σ_θ of inner layer of skirt circumference are not different among the λ curves, but do not lead into the ultimate fracture.

Stress distribution of the skirt circumference in thickness direction (σ_z, σ_r, γ_{LT}) for λ_1=1.6 when p=4.31MPa (step #80), 5.02 /597

TABLE 2 FIANL VALUES OF STRESS σ_r PERPENDICULAR TO FIBER AT SKIRT CIRCUMFERENCE (element #75) INNER LAYER.

λ_1	Ultimate burst press. MPa	σ_r at burst MPa	Fractured area
1.0	6.30	13.4	element. #5
1.2		10.7	
1.4		6.67	
1.6	6.35	8.34	element. #75
1.8	6.01	17.2	
2.0	5.86	23.3	
3.0	5.67	35.7	

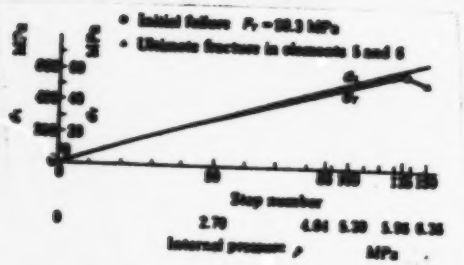

Fig. 10 Stress changes of cylindrical portion (element #5) 6th outer layer after initial failure. λ_1=1.0

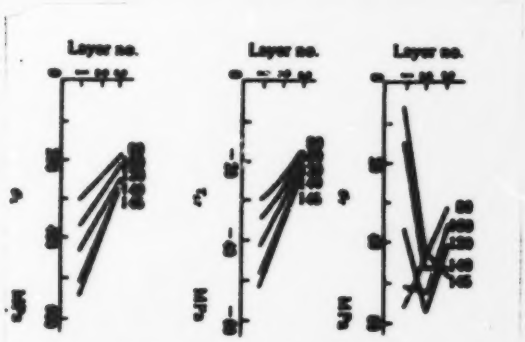

Fig. 9 Stress distributions of element #75 in the thickness direc. (λ_1=1.6)
Inner press. 4.31,5.02,5.56,6.09,6.23 MPa
Step 80,100,120,140,145

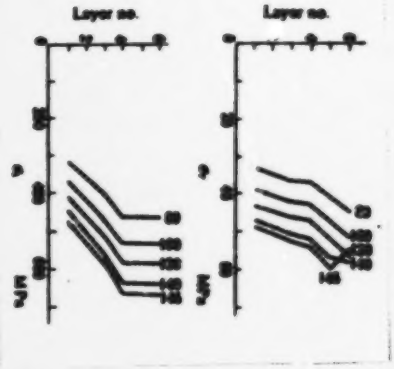

Fig. 11 Stress distributions of elem. #5 in thickness direction. (=1.0)
Inner press. 4.31,5.02,5.56,6.09,6.23MPa
Step 80,100,120,140,145

(100), 5.56 (120), 6.09 (140), 6.23 (145) are shown in Fig. 9. σ_r is unloaded at the 1st and 2nd layers in turns after the initial failure as internal pressure intensifies. σ_L and τ_{LT} is large at inner layer, and increases after σ_r's initial failure and stress re-allotment.

(4) Stress changes and distribution in thickness direction of hoop-winding reinforced outer layer after initial failure.

Stress changes of the 6th outer layer of cylindrical portion (element 5) from initial failure (p_i=5.96MPa) to ultimate fracture

ORIGINAL PAGE IS
OF POOR QUALITY

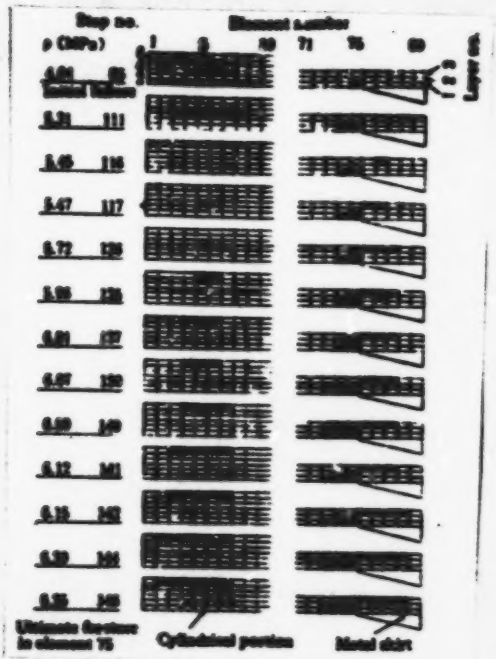

Fig. 12 Propagation of initial failure area by pressure

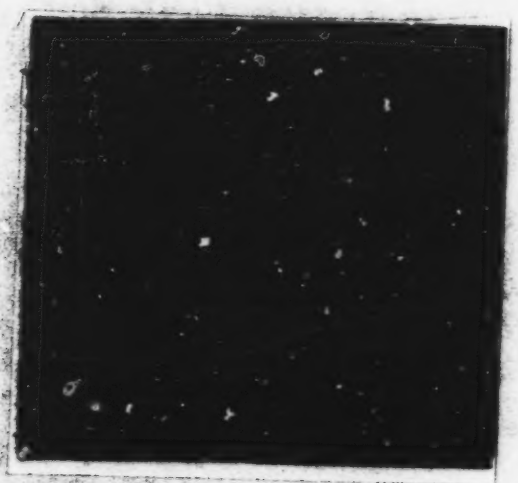

Fig. 13 CFRP rocket chamber after the burst by internal pressure.

($\beta_{\theta L}$=6.39MPa), for λ_1=1.0 is shown in Fig. 10. For λ_1=1.2-1.4, it is not much different from Fig. 10 because they are in the range where unloading does not progress well. Ultimate fracture for λ_1=1.6-3.0 occurs at the skirt circumference as seen in Fig. 8, but the stress σ_θ, σ_T of cylindrical portion (element 5) has the relationships seen in Fig. 10.

Stress distribution in thickness direction (σ_L , σ_T) of cylindrical portion (element 5) in 5 steps when internal pressure p=4.31MPa (step #80), 5.02 (100), 5.56 (120), 6.09 (140), and 6.23 (145), for λ_1=1.0 are shown in Fig. 11. 1st-3rd layers are angle-ply layers and 4th-6th layers are hoop-parallell winding layers and structually in discontinuity. σ_T is large at the outer layer (6th layer), σ_T failure starts at outer layer.

(5) Failure progress.

Fig. 12 shows the propagation where the initial failure occurs

when incremental load Δp is added. Element numbers and layer numbers are listed. There is a gap in the center because initial failure occurs at the cylindrical portion and skirt circumference area. Fig. 12 shows an example when λ_1 =1.6.

After Fr failure in the inner layer of the skirt circumference, Fr failure in the outer layer of the hoop-winding layer in the cylindrical portion occurs. When internal pressure reaches p_u =6.25MPa, fracture occurs at the skirt circumference (element 75) because of the structural unbalance. Ultimate fracture occurs after F_θ failure at the inner layer of the skirt circumference, at the cylindrical portion (element 5, 6) when λ_1 is small, at skirt circumference when λ is large.

1598

4. Comparisons of numerical calculation and internal pressure burst test results in CFRP.FW rocket chamber.

Analysis results and internal pressure test results on isotensoid curved shape CFRP rocket chamber which uses FW technique are compared (Fig. 13 fracture behavior).

4.1 Measured strain.

Mean values of surface strain ε_s and ε_θ at A, B, C, D (Fig. 3) in circumferencial direction using strain gauge are shown in O, Δ in Fig. 5 (B) and Fig. 6. In Fig. 5, it does not show much of nonlinear internal pressure-surface strain relation. Exmental values and the culculated values more or less match. In Fig. 6, experimental values at A, B, C, D is shown together with strain distribution which is obtained by calculating the 4.31MPa case. They agree well.

4.2 Burst pressure.

According to the calculation of strength using the laminate bending theory, when it reaches p_i=4.64MPa initial falure occurs at skirt circumference and propagates to the dome portion, but does not fall into ultimate fracture. Experimental values of the initial failure are not clear, but the behavior after initial failure agrees with the experimental results in which the strain and distortion increase and is making the continuous cracking sound by local failure. Next, due to the crack which is statistically distributed from the right after initial failure, the tensil stress perpendicular to the fiber and the shearing stress along the fiber rapidly falls as the failure proceeds. Therefore, Equ. (9) is used to increase λ value gradually, and numerical analysis was done for λ_1=1.0-3.0 as seen Fig. 2. As the results, as for λ_1 =1.0, 1.2, 1.4, the fracture occurs at the cylindrical portion when ultimate burst pressure reaches p =6.39MPa. As for λ_1 =1.6-3.0, the fracture occurs at skirt circumference when the pressure reaches p_b=6.25-5.47MPa. It is difficult to determine the λ curves quantatively. But ultimate burst strength depends upon λ curves.

In the experiments, the fracture occured near the metal fitting when p_u =7.46MPa (Fig. 13). It is 14% higher than the calculated burst pressure p_b=6.25MPa for λ_1=1.6. The difference of the calculated values using the quadratic function and the experimental values are due to 1: mainly assuming the curves, 2: errors of winding angles and thickness of fiber when constructed, 3: the boundary condition of the aperture, etc.

5. Closing.

In this paper, the analysis on a helical winding FW pressure vessel based on the laminate bending theory was made. The analytical method to obtain the ultimate burst strength considers geometrical and material nonlinearity based on the laminate bending theory, assumes the value that indicates the unloading behavior after the initial failure using a quadratic function. The calculations are made on the CFRP.FW rocket chamber with a sotensoid curve shape dome and are compared with the burst test. In the last paper, the general membrane theory was the base, and from the analytical value of the ultimate burst with λ =1 (decreasing stress ratio after the initial failure) is slightly higher than the experimental value. In this report, the following findings were obtained: 1: The initial failure occurs near the metal fitting which is influenced by the bending moment which occurs near the discontinuous point. The ultimate fracture sometimes occurs at the cylindrical portion and can occur near the metal fitting under the assumtion that FW laminate and the metal fitting adhere completely. They agreed with the experimental results. 2: It is difficult to quantatively determine λ value which indicates the unloading behavior after the initial falure, but since sounds of local failure were continuously heard in the experiment, with the structure of failure progress taken into consideration, it is proper to use λ curve in which λ increases as the failure progresses. The ultimate burst strength is influenced by the λ curves.

/599

REFERENCE

1) H. Iida, M. Uemura: Mechanical Characteristics of FW Pressure Vessels, Materials, 24 (1975), pp. 1044-1050.
2) H. Iida: Mechanical Characteristics of FW Pressure Vessels (Analysis of nonlinear behavior), Nihon Fukugozairyokaishi, 4 (1978), pp.163-167.
3) H. Iida::Mechanical Characteristics of FW Pressure Vessels (Nonlinear analysis with coupling effect in consideration), Nihon Kikaigaku Ronbunsyu, 47, vol. A, (1891), pp827-833.
4) H. Iida, M. Uemura: Mechanical Characteristics of FW Pressure Vessels (2nd iss.) Burst pressure with material nonlinearity in consideration, Nihon Kikaigaku Ronbunsyu, 49, vol. A, (1983), pp 1324-1333.
5) H. Fukunaga, M. Uemura, M. Iyama, H. Iida: CFRP.FW Burst Pressure on Cylindrical portions, 9th FRP Symposium Lecture Papers (1980), p.126.
6) H. Fukunaga, M. Uemura, M. Iyama, H. Iida: Strength of Laminated material (2nd iss.) Probable strength with dispersion in consideration, Papers from 22nd Lecture on Structual Strength (1980), p.96.

1600